Journal of Alloys and Compounds 504 (2010) 382–385

Contents lists available at ScienceDirect

Journal of Alloys and Compounds

journal homepage: www.elsevier.com/locate/jallcom

Hot corrosion behavior of $La_2Zr_2O_7$ with the addition of Y_2O_3 thermal barrier coatings in contacts with vanadate–sulfate salts

Zhenhua Xu[a,b,c], Limin He[a,*], Rende Mu[a], Shimei He[a], Guanghong Huang[a], Xueqiang Cao[b,**]

[a] Beijing Institute of Aeronautical Materials, Department 5, P.O. Box 81-5, Beijing 100095, China
[b] State Key Laboratory of Rare Earth Resource Utilization, Changchun Institute of Applied Chemistry, Chinese Academy of Sciences, Changchun 130022, China
[c] Graduate School of Chinese Academy of Sciences, Beijing 100039, China

ARTICLE INFO

Article history:
Received 30 April 2010
Received in revised form 10 May 2010
Accepted 21 May 2010
Available online 4 June 2010

Keywords:
Thermal barrier coatings
EB-PVD
Hot corrosion
$La_2Zr_2O_7$
Y_2O_3

ABSTRACT

Thermal barrier coatings (TBCs) of $La_2Zr_2O_7$ with the addition of 3 wt.% Y_2O_3 (LZ3Y) were deposited by electron beam-physical vapor deposition (EB-PVD). The phase structure, surface morphology, hot corrosion behavior of the LZ3Y coating was studied in detail. The present study investigates the hot corrosion performance of LZ3Y coating in the presence of molten mixture of $Na_2SO_4 + V_2O_5$ at 1173 K for 100 h. X-ray diffraction (XRD) indicates that the chemical reaction between $NaVO_3$ and LZ3Y produces $LaVO_4$, YVO_4 and *m*-ZrO_2, leaching La_2O_3 and Y_2O_3 from LZ3Y and causing the progressive destabilization transformation from *t*′ to *m*-ZrO_2. The excess La_2O_3 in the as-deposited LZ3Y coating can largely aggravate the degradation of LZ3Y coating by both $NaVO_3$ and Na_2SO_4, resulting in very rapid disintegration of the coating. Phase transformation and chemical interaction are the primarily corrosive mechanisms for deterioration of LZ3Y coating.

1. Introduction

Electron beam-physical vapor deposited (EB-PVD) thermal barrier coatings (TBCs) are widely used to protect the hot-section parts of aircraft engine turbines, because the segmented columnar structure of EB-PVD TBCs induces high strain compliance [1,2]. Up to now, the most successful TBC materials are 6–8 wt.% yttria stabilized zirconia (YSZ) [3]. However, a major disadvantage of YSZ is the limited operation temperature of 1473 K for long-term application due to serious phase transformation and sintering, which will generate to the spallation failure of TBCs [3–5].

In the next generation of advanced engines, further increases in thrust-to-weight ratio will require even higher gas temperature. This means that higher surface temperatures and larger thermal gradients are expected in advanced TBCs as compared with the conventional YSZ TBCs [6]. In recent years, the rare earth zirconates have been investigated and the results indicate these materials are significant for the top ceramic materials for future TBCs [1–8]. Especially those materials with the pyrochlore structures, $La_2Zr_2O_7$ with the addition of 3 wt.% Y_2O_3 (LZ3Y) shows promising thermophysical properties and has attracted a great attention [9,10].

On the other hand, TBCs are also finding increasing application in engines for marine applications that are usually operated in corrosive environments or burn low-quality fuels containing impurities such as vanadium, sulfur and sodium. In this case, another failure mode, hot corrosion, becomes predominant and crucial to the lifetime of TBCs [11,12]. The porous columns and inter-columnar gaps intrinsic in EB-PVD ceramic top coat provide penetration paths for molten salts such as vanadates and sulfates, to attack the EB-PVD TBC systems. Therefore, hot corrosion resistance over extended exposures in low-quality fuel combustion or corrosive environments is another key durability issue for expansive application of EB-PVD TBCs [13].

Up to date, no data on the phase evolution and microstructure change of LZ3Y EB-PVD TBCs upon high temperature exposure to molten vanadate–sulfate salts is available in open literatures. In the present work, the LZ3Y coating samples are exposed to a molten mixture of $V_2O_5 + Na_2SO_4$ for a period of 100 h at 1173 K, and the corrosive mechanisms are also studied.

2. Experimental procedure

LZ3Y powder with the desired composition was synthesized by solid-state reaction at 1673 K for 12 h with La_2O_3, ZrO_2 and Y_2O_3 as the starting materials. After the cast-formation, the ingot was densified at 1773 K for 12 h. The directionally solidified Ni-based superalloy DZ125 (30 mm × 10 mm × 1.5 mm) was used as the substrate material. The substrate was ground before the bond coat (BC) of NiCrAlYSi was deposited by arc ion-plating (A-1000 Unit). After the deposition of BC, the substrates were heat-treated under high vacuum at 1143 K for 3 h. The purpose of heat treatment at 1143 K before EB-PVD deposition was to enhance the adhesion of bond coat

* Corresponding author. Tel.: +86 10 62496456; fax: +86 10 62496456.
** Corresponding author. Tel.: +86 431 85262285; fax: +86 431 85262285.
E-mail addresses: he_limin@yahoo.com (L. He), xcao@ciac.jl.cn (X. Cao).

0925-8388/$ – see front matter © 2010 Published by Elsevier B.V.
doi:10.1016/j.jallcom.2010.05.121

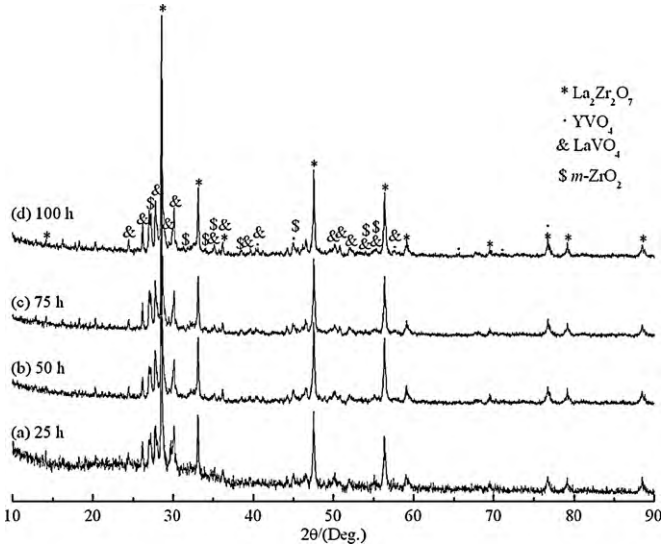

Fig. 1. XRD patterns of the LZ3Y coating after different hot corrosion durations: (a) 25 h, (b) 50 h, (c) 75 h and (d) 100 h.

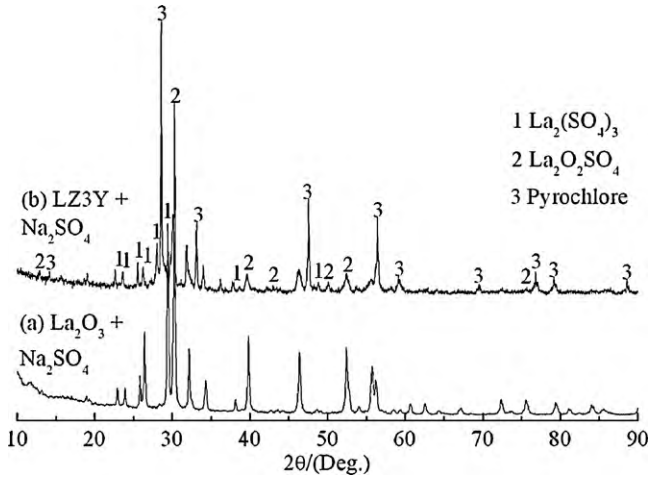

Fig. 2. XRD patterns of the mixtures after being heated at 1173 K for 100 h: (a) La_2O_3 and Na_2SO_4, (b) LZ3Y and Na_2SO_4. "3" labeled in (b) represents "Pyrochlore" structure.

to substrate due to interdiffusion between them. The top ceramic coat of LZ3Y was fabricated by EB-PVD. The current of electron beam was in the range of 550–700 mA. Meanwhile, the accelerated high-voltage (kV) was in the range of −9.58 to −10.14.

The 40 wt.% V_2O_5 + 60 wt.% Na_2SO_4 mixture were applied uniformly over the LZ3Y coatings surface to a coverage of 10 mg cm^{-2}. Then the specimens were isothermally heated at 1173 K in an air furnace for 100 h. Meanwhile, after the isothermal oxidation for a certain time, some selected specimens were removed out for further microstructure analyses. Upon heating, the salt mixture was molten on the coatings surface. Following a 100 h dwelling, the specimens were furnace-cooled down to room temperature.

Scanning electron microscope (SEM, FEI-Quanta 600) equipped with energy dispersive spectroscopy (EDS, Oxford INCAx-sight 6427) was applied for the microstructure and composition evaluation. The VHX-100 (Keyence) digital video microscope equipped with three-dimensional (3D) image feature was used to obtain information on the surface morphologies of the coatings after hot corrosion, as well as the size and depth arising from the corrosive pores. X-ray diffraction (XRD, Bruker D8 Advance) with Cu-K_α radiation at a scan rate of 8° min^{-1} was employed to analyze the phase structural evolution of the hot corrosion products.

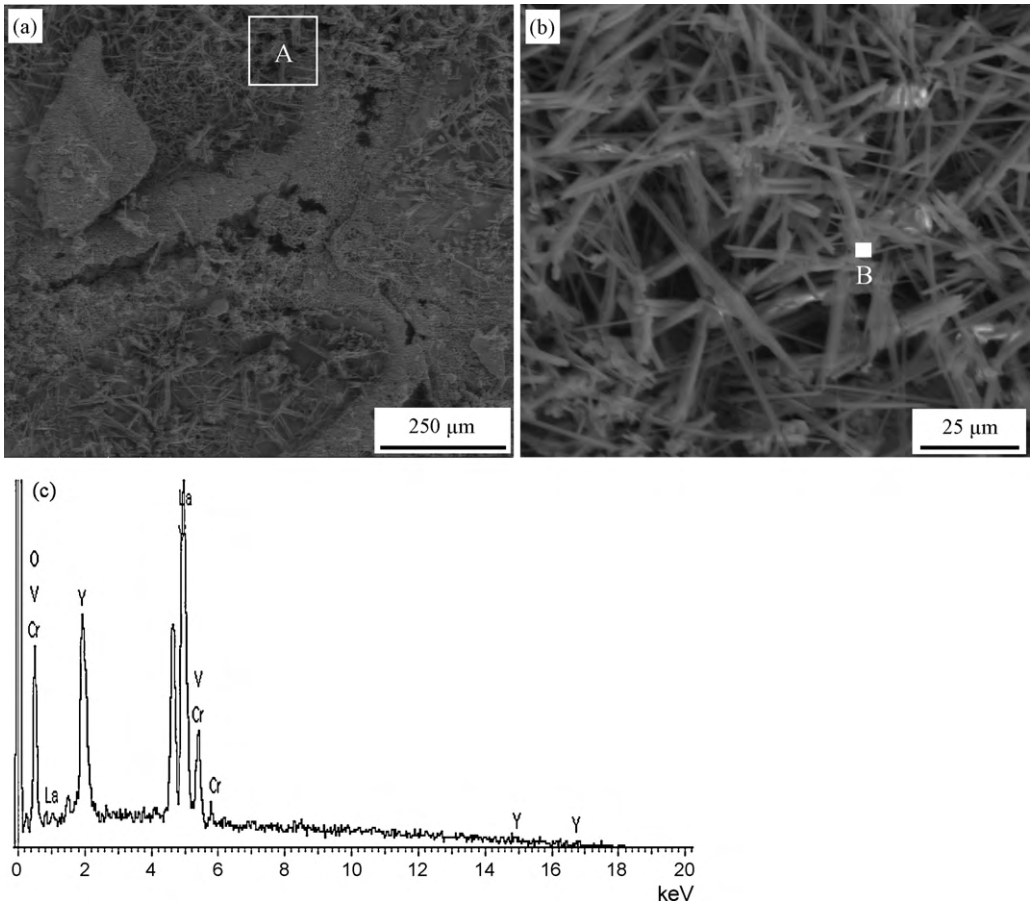

Fig. 3. SEM surface morphology of the (a) LZ3Y coating after exposure of 100 h; (b) is the enlarged image of area "A" in (a); (c) represents EDS spectrum of area "B" in (b).

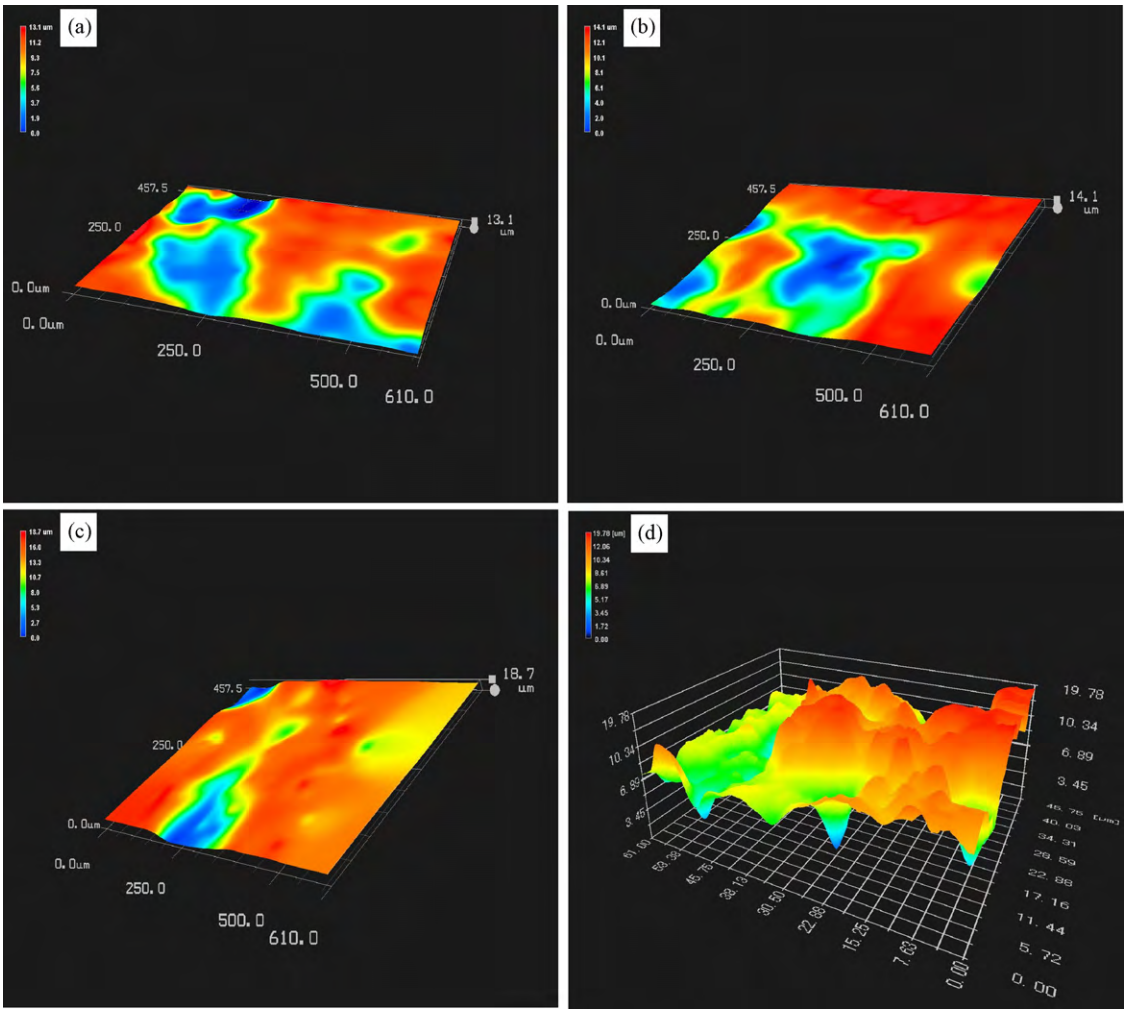

Fig. 4. 3D surface morphologies of the (a) LZ3Y coatings after different hot corrosion durations: (a) 25 h, (b) 50 h, (c) 75 h and (d) 100 h.

3. Results and discussion

The XRD patterns of LZ3Y coating after hot corrosion for different exposure periods are compiled in Fig. 1. Exposure of the LZ3Y coating to a molten mixture of $Na_2SO_4 + V_2O_5$ at 1173 K results in additional peaks attributed to $LaVO_4$, YVO_4 and *m*-ZrO_2 together with the original pyrochlore ($La_2Zr_2O_7$) peaks. The possible mechanisms that would have produced these phases can be written as [14]:

$$Na_2SO_4(l) \rightarrow Na_2O(l) + SO_3(g) \quad (1)$$

$$Na_2O(l) + V_2O_5(l) \rightarrow 2NaVO_3(l) \quad (\text{meltingpoint} : 883\,\text{K}) \quad (2)$$

$$La_2O_3(s) + 2NaVO_3(l) \rightarrow 2LaVO_4(s) + Na_2O(l) \quad (3)$$

$$La_{2-2x}Y_{2x}Zr_2O_7(s) + 2NaVO_3(l) \rightarrow 2-2xLaVO_4(s) + 2xYVO_4(s) + 2m\text{-}ZrO_2(s) + Na_2O(l) \quad (4)$$

Due to the significant existence of the original pyrochlore peaks following 100 h of exposure, reactions (2) and (3) may be the main mechanisms responsible for the occurrence of $LaVO_4$ and YVO_4 phases. In other words, LZ3Y material is relatively resistant to attack by V_2O_5.

As previously reported by Marple et al. [15], $La_2Zr_2O_7$ coating prepared by plasma spraying was easy to attack by Na_2SO_4 at 1000 °C. In order to examine whether the chemical interaction between LZ3Y coating and Na_2SO_4, a mixture of La_2O_3 and Na_2SO_4 (or LZ3Y and Na_2SO_4) powders in a molar ratio of 1:3 was heated at 1173 K for 100 h, and the XRD results are shown in Fig. 2. Obviously, after being heated treatment for 100 h, the oxysulfate ($La_2O_2SO_4$) together with few of $La_2(SO_4)_3$ phases are detected in Fig. 2a and b. The possible reactions that would have produced $La_2O_2SO_4$ and $La_2(SO_4)_3$ phases can be expressed as:

$$2La_2O_3(s) + 5Na_2SO_4(l) \rightarrow La_2O_2SO_4(s) + La_2(SO_4)_3(s) + SO_3(g) + 5Na_2O(l) \quad (5)$$

$$2La_2Zr_2O_7(\text{inLZ3Y})(s) + 6Na_2SO_4(l) \rightarrow La_2O_2SO_4(s) + La_2(SO_4)_3(s) + 4m\text{-}ZrO_2(s) + 2SO_3(g) + 6Na_2O(l) \quad (6)$$

It has been reported that at these temperatures (1173 K) the oxysulfate rather than the sulfate, $La_2(SO_4)_3$, is the dominant species [15,16]. Hence LZ3Y coating with excess La_2O_3 is rapidly degraded when exposed to sulfur-containing compounds at 900 °C even though the mechanism behind could not be fully identified.

As expected, any reaction products of molten $Na_2SO_4 + V_2O_5$ with ZrO_2 from the XRD patterns are not be detected after hot corrosion. This could be explained based on the thermal instability of ZrV_2O_7. Below 1020 K, molten $NaVO_3$ produced from reaction (2) first reacts with LZ3Y to form $LaVO_4$, YVO_4, ZrV_2O_7 and Na_2O. The reaction mechanism below 1020 K is given by the following

chemical equation:

$$La_{2-2x}Y_{2x}Zr_2O_7(s) + 6NaVO_3(l) \rightarrow 2-2xLaVO_4(s) + 2xYVO_4(s) + 2ZrV_2O_7(s) + 3Na_2O(l) \quad (7)$$

According to the phase diagram in the ZrO_2–V_2O_5 binary system, ZrV_2O_7 is the only existent compound in this system. At about 1020 K, ZrV_2O_7 melts incongruently to *m*-ZrO_2 and a liquid mixture of *m*-ZrO_2 and V_2O_5 [12,17,18]. Above 1020 K, i.e., 1173 K in this study, molten V_2O_5 from the incongruent melting of ZrV_2O_7 reacts with Na_2O to form $NaVO_3$, which further reacts with LZ3Y to form $LaVO_4$, YVO_4, ZrV_2O_7 and Na_2O, as shown in Eq. (7). At the same time, ZrV_2O_7 melts incongruently to *m*-ZrO_2 and a liquid mixture of *m*-ZrO_2 and V_2O_5. This process is repeated until V_2O_5 is finally depleted, and the final reaction products are $LaVO_4$, YVO_4, *m*-ZrO_2 and Na_2O.

Fig. 3 shows the SEM surface morphology of the LZ3Y coating after hot corrosion and corresponding EDS analysis. The LZ3Y coating has experienced severe cracking and delamination. Especially those corrosive pores are apparent seen in Fig. 3a, which can further contribute to the deterioration of the coating. Both chemical interaction (Eqs. (4) and (6)) and phase transformation are the main reasons for the serious cracking and spallation. Additionally, the generation of thermo-mechanical stress due to solidification of corrosive melts may be responsible for the occurrence of some microcracks on the coating surface. It is interesting to see from Fig. 3b that $LaVO_4$ and YVO_4 crystals as evidenced by EDS and XRD (Figs. 1d and 3c) with elongated and thread-like structures varying in sizes up to 1.5 μm width are found to be evenly spread on the coating surface, it may be induced by the outward diffusion of La^{3+} and Y^{3+}. The La^{3+} and Y^{3+} in the lattices have the mobility to migrate preferentially toward the reaction interfaces due to the high V concentration present on the coating surface. Additionally, $LaVO_4$ and YVO_4 crystals detected in area "B" is a composite of three phases, of which few of Cr_2O_3 phases is simultaneously included. The pattern of grain growth is probably related to the inclusion of the second phase. Inclusions with a different size can be used to control the grain growth, and this can be introduced by mixing multi-phase corrosive melts [19].

Fig. 4 shows the 3D images of surface morphologies of the LZ3Y coatings after hot corrosion for different exposure periods. Obviously, the surface morphologies of LZ3Y coatings look coarse and have experienced severe attack. Therefore, the depth of the corrosive pores occurred in LZ3Y coatings increases with the dwelling time (from 13.1 to 19.78 μm). For the number of corrosive pores, the situation is identical. Herein it is worth emphasizing that the chemical interaction between the LZ3Y specie and molten mixture of $Na_2SO_4 + V_2O_5$ is the important factor resulting in degradation of the coating. Especially the excess of La_2O_3 contained in the as-deposited LZ3Y coating has the disruptive effect on the integrity of the coating. Because the pyrochlore structure exists stably in a rather large range of La/Zr molar ratio from 0.87 to 1.15 according to the phase diagram of La_2O_3–ZrO_2 [20,21]. La^{3+} (0.116 nm) has a larger ionic radius than Y^{3+} (0.101 nm) and Zr^{4+} (0.072 nm). The lager is the ionic radius, the stronger is the relative basicity. La_2O_3 with the stronger basicity will react severely with the highly molten mixture of $Na_2SO_4 + V_2O_5$. In general, chemical interactions between zirconia-based TBCs and a molten oxide can degrade the coating, the severity of which increases as the relative acidity to basicity between the two materials increases. The reaction between V_2O_5 and metal oxides like La_2O_3, Y_2O_3 and ZrO_2 has been proposed to follow a Lewis acid–base mechanism [18]. Thus, metal oxides with the strongest basicity will react most severely with the highly acidic V_2O_5. Since the basicity of La_2O_3 is high relative to the Y_2O_3 and ZrO_2 (e.g. $La_2O_3 > Y_2O_3 > ZrO_2$), it is reasonable to consider that the molten mixture of $Na_2SO_4 + V_2O_5$ aggressively attacks the La_2O_3.

4. Conclusions

LZ3Y coating prepared by EB-PVD is relatively resistant to attack by V_2O_5, but it has experienced severe cracking and delamination when in contacts with molten mixture of $Na_2SO_4 + V_2O_5$. Hence it is reasonable to suggest that the deposition condition of LZ3Y coating should be properly controlled to keep the content of excess La_2O_3 as low as possible. Additionally, some protective techniques could be used to seal the top coat surface and further prevent the penetration of molten salts into the porous LZ3Y EB-PVD TBCs.

Acknowledgements

Financial supports from projects NSFC-50825204, NSFC-20921002 and Hunan Provincial Key Laboratory of Materials Protection for Electric Power and Transportation (Changsha University of Science & Technology) are also gratefully acknowledged.

References

[1] X.H. Zhong, Z.H. Xu, Y.F. Zhang, J.F. Zhang, X.Q. Cao, J. Alloy Compd. 469 (2009) 82–88.
[2] Y.H. Wang, J.H. Ouyang, Z.-G. Liu, J. Alloy Compd. 485 (2009) 734–738.
[3] Z.-G. Liu, J.H. Ouyang, Y. Zhou, J. Alloy Compd. 473 (2009) L17–L19.
[4] Z.-G. Liu, J.H. Ouyang, B.H. Wang, Y. Zhou, J. Li, J. Alloy Compd. 466 (2008) 39–44.
[5] Z.-G. Liu, J.H. Ouyang, Y. Zhou, J. Alloy Compd. 472 (2009) 319–324.
[6] Z.-G. Liu, J.H. Ouyang, Y. Zhou, J. Li, J. Alloy Compd. 468 (2009) 350–355.
[7] H.F. Chen, Y.F. Gao, Y. Liu, H.J. Luo, J. Alloy Compd. 480 (2009) 843–848.
[8] H.F. Chen, Y.F. Gao, S.Y. Tao, Y. Liu, H.J. Luo, J. Alloy Compd. 486 (2009) 391–399.
[9] Z.H. Xu, L.M. He, R.D. Mu, S.M. He, X.Q. Cao, J. Alloy Compd. 492 (2010) 701–705.
[10] Z.H. Xu, L.M. He, X.H. Zhong, J.F. Zhang, X.L. Chen, H.M. Ma, X.Q. Cao, J. Alloy Compd. 480 (2009) 220–224.
[11] S.H. Cho, J.M. Hur, C.S. Seo, J.S. Yoon, S.W. Park, J. Alloy Compd. 468 (2009) 263–269.
[12] X.H. Zhong, Y.M. Wang, Z.H. Xu, Y.F. Zhang, J.F. Zhang, X.Q. Cao, Mater. Corros. 60 (2009) 882–888.
[13] X.H. Zhong, Y.M. Wang, Z.H. Xu, Y.F. Zhang, J.F. Zhang, X.Q. Cao, J. Eur. Ceram. Soc. 30 (2010) 1401–1408.
[14] P. Mohan, B. Yuan, T. Patterson, V.H. Desai, Y.H. Sohn, J. Am. Ceram. Soc. 90 (2007) 3601–3607.
[15] B.R. Marple, J. Voyer, M. Thibodeau, D.R. Nagy, R. Vassen, J. Eng. Gas Turb. Power 128 (2006) 144–152.
[16] J.A. Poston, R.V. Siriwardane, E.P. Fisher, A.L. Miltz, Appl. Surf. Sci. 214 (2003) 83–102.
[17] Z.-G. Liu, J.H. Ouyang, Y. Zhou, J. Li, X.L. Xia, J. Eur. Ceram. Soc. 29 (2009) 647–652.
[18] Z. Chen, S. Speakman, J. Howe, H. Wang, W. Porter, R. Trice, J. Eur. Ceram. Soc. 29 (2009) 1403–1411.
[19] X.Q. Cao, J.Y. Li, X.H. Zhong, J.F. Zhang, Y.F. Zhang, R. Vassen, D. Stover, Mater. Lett. 62 (2008) 2667–2669.
[20] J. Wang, S.X. Bai, H. Zhang, C.R. Zhang, J. Alloy Compd. 476 (2009) 89–91.
[21] H.M. Zhou, D.Q. Yi, Z.M. Yu, L.R. Xiao, J. Alloy Compd. 438 (2007) 217–222.